



# High-resolution Infrared Spectroscopy and analysis of the $\nu_2$ / $\nu_4$ bending dyad of Ruthenium Tetroxide

S. Reymond-Laruinaz, M. Faye, V. Boudon, D. Doizi, L. Manceron

## ► To cite this version:

S. Reymond-Laruinaz, M. Faye, V. Boudon, D. Doizi, L. Manceron. High-resolution Infrared Spectroscopy and analysis of the  $\nu_2$  /  $\nu_4$  bending dyad of Ruthenium Tetroxide. Journal of Molecular Spectroscopy, 2017, 10.1016/j.jms.2017.04.010 . hal-01509861

**HAL Id: hal-01509861**

**<https://hal.sorbonne-universite.fr/hal-01509861>**

Submitted on 18 Apr 2017

**HAL** is a multi-disciplinary open access archive for the deposit and dissemination of scientific research documents, whether they are published or not. The documents may come from teaching and research institutions in France or abroad, or from public or private research centers.

L'archive ouverte pluridisciplinaire **HAL**, est destinée au dépôt et à la diffusion de documents scientifiques de niveau recherche, publiés ou non, émanant des établissements d'enseignement et de recherche français ou étrangers, des laboratoires publics ou privés.

# High-resolution Infrared Spectroscopy and analysis of the $\nu_2/\nu_4$ bending dyad of Ruthenium Tetroxide

S. Reymond-Laruinaz<sup>1</sup>; M. Faye<sup>2</sup>; V. Boudon<sup>3</sup>; D. Doizi<sup>1</sup>; L. Manceron<sup>2,4</sup>

<sup>1</sup>Den-SERVICE d'Etude du Comportement des Radionucléides (SECR), CEA, Université Paris-Saclay, F-91191, Gif-sur-Yvette, France,

<sup>2</sup>Synchrotron SOLEIL, AILES Beamline, L'Orme des Merisiers, St-Aubin BP48, 91192 Cedex, France,

<sup>3</sup>Laboratoire Interdisciplinaire Carnot de Bourgogne, UMR 6303 CNRS-Université Bourgogne Franche-Comté, 9 avenue Alain Savary, BP 47870, F-21078 Dijon Cedex, France,

<sup>4</sup>MONARIS, UMR 8233, Université Pierre et Marie Curie, 4 Place Jussieu, case 49, F-75252 Paris Cedex 05, France.

## Abstract

$\text{RuO}_4$  is a heavy tetrahedral molecule of interest in several fields. Due to its chemical toxicity and radiological impact of its 103 and 106 isotopologues, the possible remote sensing of this compound in the atmosphere has renewed interest in its spectroscopic properties. We investigate here, for the first time at high resolution, the bending modes region in the far infrared. High resolution FTIR spectra have been recorded near room temperature, using a specially designed cell and an isotopically pure sample of  $^{102}\text{RuO}_4$ . New assignments and effective Hamiltonian parameter fits for the main isotopologue ( $^{102}\text{RuO}_4$ ) have been performed, treating the whole  $\nu_2/\nu_4$  bending mode dyad. We provide precise effective Hamiltonian parameters, including band centers and Coriolis interaction parameters.

## Keywords

Ruthenium Tetroxide - High resolution FTIR spectroscopy – Simulation – Isotopic shift

## 1. Introduction

Ruthenium tetroxide ( $\text{RuO}_4$ ) is one of the few neutral tetroxide species. It is a heavy tetrahedral molecule, but is relatively volatile with a notable vapor pressure at room temperature. It is also a powerful oxidant and can be used in oxidation reactions [1, 2].  $\text{RuO}_4$  is quite reactive at room temperature and decomposes readily to produce  $\text{RuO}_2$  films, which is used in the semiconductor industry [3]. Ru is also a fission product of uranium and can be created, under its volatile form  $\text{RuO}_4$ , after an air inlet in the nuclear containment and can be used as a marker of air ingress in the reactor during a severe nuclear accident [4-6]. For this reason, the possible remote sensing of this compound in the atmosphere has gained technological importance and motivated recent spectroscopic studies [7]. Besides this interest motivated by nuclear reactor technology, detailed studies of  $\text{RuO}_4$  high resolution FTIR absorption spectrum present an interest for quantum chemistry, as it would provide vibrational and structural parameters as benchmarks for the modeling of heavy element compounds [8-14].

For the low frequency bending modes, only low resolution vibrational studies of  $\text{RuO}_4$  in the vapor (IR) or condensed (Raman) phases [15, 16] exist. These have, from band shape studies and force fields, approximately estimated band center positions, as well as rotational and Coriolis constants. These studies have been used ever since as benchmarks for *ab initio* calculations of vibrational properties [11-14].

Up to now, only the strongly IR-active,  $\nu_3$  stretching fundamental has been investigated at high-resolution ( $0.001\text{ cm}^{-1}$ ) and rotationally analyzed as an isolated band [7,17], with help of a  $^{102}\text{Ru}$ -sample. Analysis of the rotational structure was made possible by the fact that oxygen atoms have no nuclear spin, implying that only  $A_1$  and  $A_2$  rovibrational levels are allowed, which makes the  $\text{RuO}_4$  spectrum rotationally resolvable as, here, most rotational lines are isolated. Natural abundance ruthenium has seven isotopes:  $^{104}\text{Ru}$  (18.7%),  $^{102}\text{Ru}$  (31.6%),  $^{101}\text{Ru}$  (17.0%),  $^{100}\text{Ru}$  (12.6%),  $^{99}\text{Ru}$  (12.7%),  $^{98}\text{Ru}$  (1.88%),  $^{97}\text{Ru}$  (5.52%) and, thus, use of an enriched  $^{102}\text{RuO}_4$  sample is necessary. An experimental high resolution study of  $\text{RuO}_4$  in the far infrared is a specially challenging task and several difficulties must be overcome: the molecule is reactive and a special procedure must be used for the synthesis and handling of an isotopically enriched sample.

In this paper, we present new experimental results, using Synchrotron Radiation (SR) coupled to a high resolution FTIR spectrometer and a new long path cell made of inert materials to study the vibrational spectra of  $\text{RuO}_4$ . High resolution ( $0.001\text{ cm}^{-1}$ ) spectra of the  $\nu_2/\nu_4$  region of pure  $^{102}\text{RuO}_4$  have been recorded. Using the tensorial formalism and methods developed previously [18-21], spectra are analyzed in detail and compared to its heavier analogue, osmium tetroxide [22-24]. Assignments are performed up to high  $J$  rotational quantum number values. In Section 2 we present the experimental details of the FTIR spectra acquisitions. Section 3 recalls the basics of the theoretical model used for spherical-top molecules. We present the results of the analysis and discuss them in Section 4.

## 2. Experimental details and results

*Sample preparation and handling.*  $\text{RuO}_4$  and a monoisotopic  $^{102}\text{RuO}_4$  sample have been prepared using the method of Ruff and Vidic [25], starting from Ru powder (Aldrich, 99.9%) or  $^{102}\text{Ru}$  (Eurisotop, 99.8% enrichment), oxidized first to perruthenate by permanganate using alkaline fusion and, next, partly reduced in acidic solution. To eliminate unwanted impurities (water, carbon dioxide, etc), a slight variant in the preparation involved flowing the product from the warmed solution with dry nitrogen gas for trapping and distillation of the product over dried and outgassed magnesium perchlorate-filled traps to remove water condensate. Carbon dioxide traces were eliminated by pumping over the product maintained in a cold bath around  $-35^\circ\text{C}$ . All preparative glassware must be completely grease-free, with Teflon™ seals and stopcocks. The products were kept in sealed glass flasks over magnesium perchlorate outgassed at  $200^\circ\text{C}$  in high vacuum. The sample was handled using equipment and handling procedures as described in [7].

Because of the weakness of the IR absorption in the bending mode region, a new, long path cell was designed in a simple White-configuration. As  $\text{RuO}_4$  progressively decomposes in contact with metal or oxidizable surfaces, a special gas cell was made of glass for the cell cylindrical body, Teflon™ bellows for mirror steering or PTFE-coated aluminum alloy for the flanges. The cell was fitted with wedged KRS5 windows mounted with Teflon™-coated silicone or Kalrez gaskets (Eriks, France). A triple-envelope glass cell body has been manufactured (Verrerie Soufflée Normalisée, Paris, France) with an inner volume of about 14 liters (15 cm ID  $\times$  80 cm length) surrounded by an annular cylindrical space for circulating a cooling gas and a third envelope for keeping an insulating vacuum (Figure 1). The metal flanges supporting the windows, mirror mounts and viewports were covered with a thick PTFE coating (STIM, Cachan, France) and the mirrors were mounted on Teflon™ bellows (Elkinger, Germany) allowing for travel and tilt adjustments.

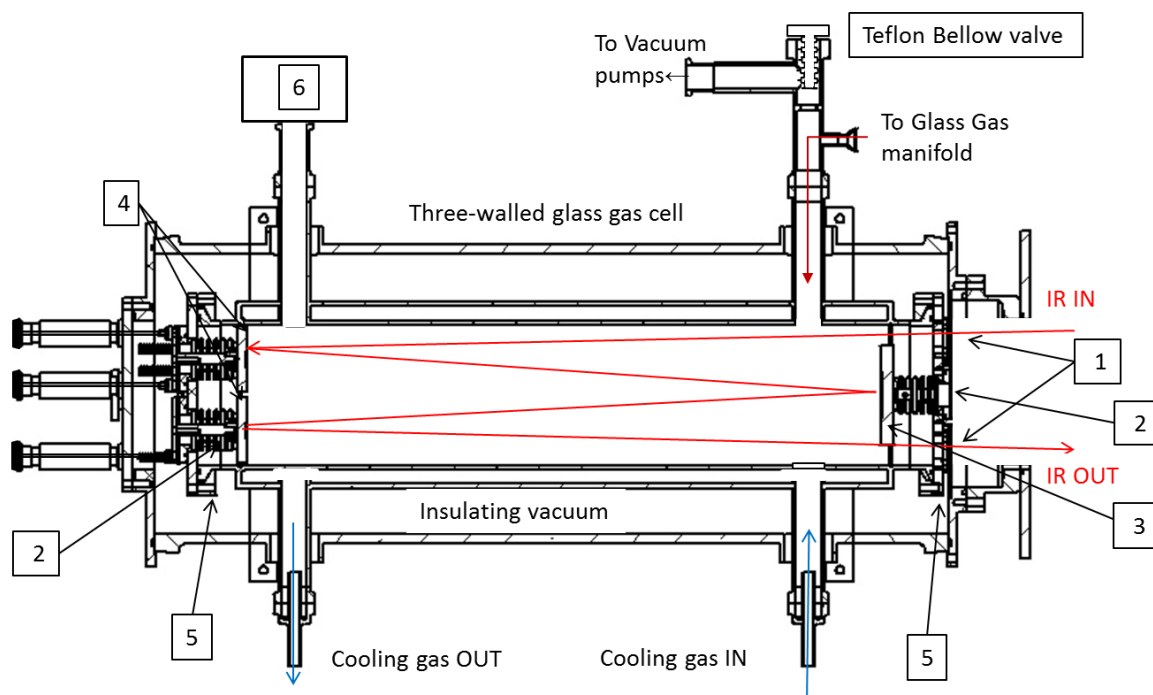


Figure 1. Schematic View cut of the glass and Teflon multi pass cell built for the experiment. 1- Wedged KRS5 windows. 2- Teflon Bellows. 3- Field mirror. 4- Objective Mirrors. 5- PTFE-coated flanges. 6- Passivated capacitance Pressure Gauge [7].

After various trials, it was found that gold coated-mirrors passivated with a thin, sub-micron homogeneous alumina layer (OPTIMASK, Morangis, France) could be used without catalyzing sample decomposition. The cell has an optical base length of 0.68m and a volume of about 14 liters. The optical path length can be varied between about 2.80 and 42 m. As in ref. 7, the cell and gas manifold were treated with a low pressure oxygen discharge and ozone to clean and passivate surfaces in contact with the gas. After four days in the cell, the product loss was about 30%.

The cell is coupled to the side compartment of the IFS 125HR (Bruker, Germany) of the AILES beamline, so that the insulating vacuum insulating the inner cell is that of the spectrometer. With two magnetic bearing turbopumps in operation, the residual vacuum (ca  $5 \times 10^{-5}$  mbar) was good enough for our purpose. The infrared beam was extracted from and redirected into the spectrometer sample compartment with an f/12 transfer optics, to match the f/10 cell mirror optical aperture without risk of vignetting the IR beam.

**Spectroscopic measurements.** The experiments were carried out on the AILES Beamline of synchrotron Soleil, with the IFS 125 Bruker interferometer coupled to the SR source. Two spectra were recorded, one with 5.44 m and 0.2 mbar sample pressure and a second with 19.04 m path length and the same pressure for a better recording of the weaker lines. The resolution used was  $0.00102 \text{ cm}^{-1}$  (Bruker definition,  $\text{Res} = 0.9/\text{MOPD}$ , where  $\text{MOPD} = 882\text{cm}$ ) with no apodization ("boxcar" software option), 5.06 cm/s scanner velocity, a Si/6 $\mu\text{m}$  Mylar beamsplitter and a liquid Helium-cooled Bolometer, using a  $650 \text{ cm}^{-1}$  low-pass filter. For each spectrum 296 and 240 interferograms, respectively, were averaged in a total recording time of about 27 hours and processed against a background of the empty cell taken at the same temperature at  $0.1 \text{ cm}^{-1}$  resolution. Another spectrum was recorded at  $0.0025\text{cm}^{-1}$  resolution with natural  $\text{RuO}_4$ , using the Globar source of the spectrometer, 570 interferograms were averaged over about 30 hours measurement time, corresponding to two refills of the cell with a pressure of about 0.13 mbar.

Spectra were zero-filled, corrected for channelling effects and calibrated using well-known H<sub>2</sub>O and CO<sub>2</sub> rotational lines [27].

*Experimental results.* Figure 2 presents a survey of the whole bending region, recorded with a moderate  $0.2 \times 544$  mbar.cm pressure  $\times$  optical path length product. Note that the product decays slowly during the experiment. After passivation, the half-life is more than 96 h.

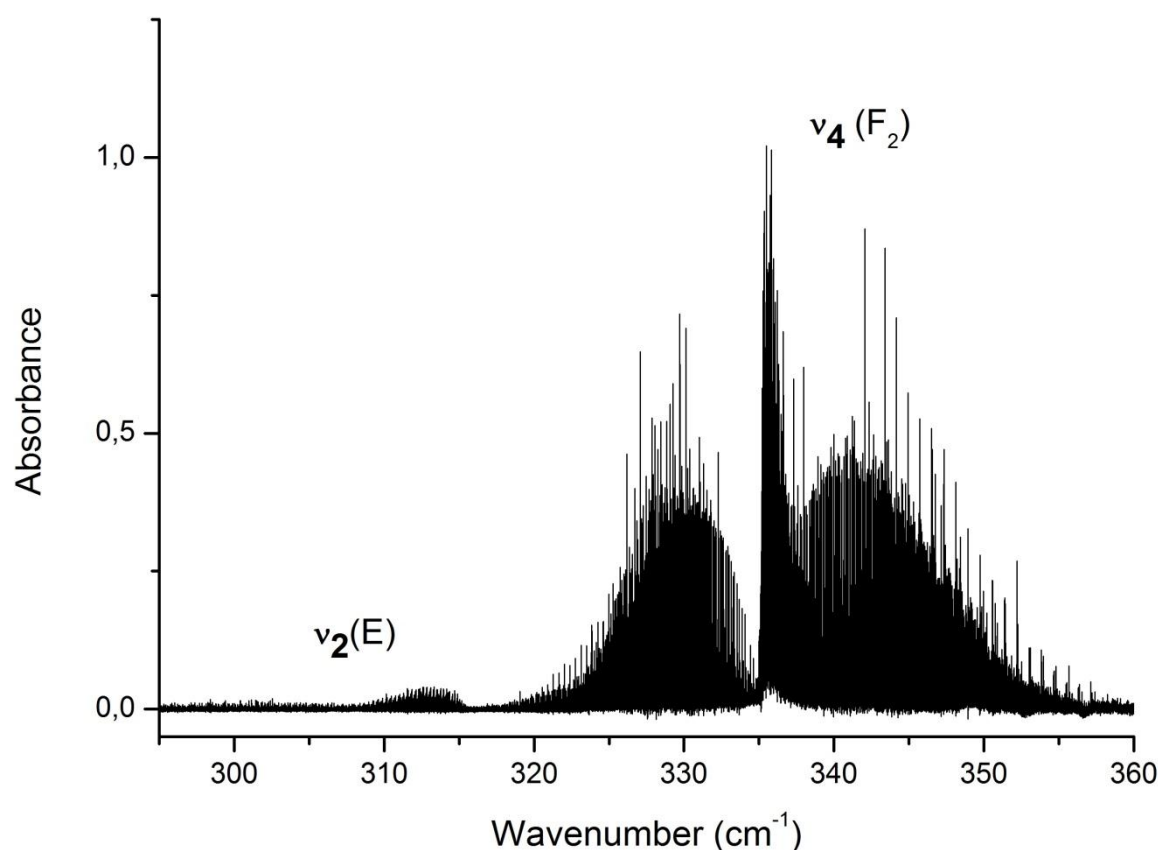


Figure 2. Survey of the 300-360 cm<sup>-1</sup>  $v_2/v_4$  bending region of <sup>102</sup>RuO<sub>4</sub> for a sample pressure of about 0.20 mbar and a path length of 5.44m, Residual water vapor lines have been subtracted out for clarity.

### 3. Theoretical model

RuO<sub>4</sub>, like other tetrahedral spherical top molecules ( $T_d$  point group), possesses four normal modes of vibration: one non-degenerate mode with  $A_1$  symmetry ( $v_1$ ), one doubly degenerate mode with  $E$  symmetry ( $v_2$ ), and two triply degenerate modes with  $F_2$  symmetry ( $v_3$  and  $v_4$ ). Only  $F_2$  fundamentals are infrared active, in a first approximation, but the other modes can gain some absorption intensity through couplings with the  $F_2$  modes. If the  $v_1$  and  $v_3$  stretching fundamental wavenumbers are relatively far apart (885.0 and 921.0 cm<sup>-1</sup>, respectively, for <sup>102</sup>RuO<sub>4</sub>, see ref. 7), the  $v_2$  and  $v_4$  bending fundamental wavenumbers are much closer to each other and both are located in the far infrared region (about 314 and 336 cm<sup>-1</sup>, respectively [16]). It is obvious from the spectrum that the  $v_2$  mode gains substantial IR intensity from the neighboring  $F_2$  mode, which is possible through Coriolis coupling. This leads to a vibrational dyad structure that will be discussed later.

The theoretical model described below to develop the Hamiltonian operator is based on the tensorial formalism and vibrational extrapolation methods used in Dijon. These methods have already been

explained for example in Refs. [18, 19, 21]. Only the basic principles and their application to the case of a tetrahedral molecule are recalled here.

If we consider an  $XY_4$  molecule for which the vibrational levels are grouped into a series of polyads designed by  $P_k$  ( $k=0, \dots, n$ ),  $P_0$  being the ground state (GS), the Hamiltonian operator can be put in the following form (after performing some contact transformations):

$$H = H_{\{P_0 \equiv GS\}} + H_{\{P_1\}} + \dots + H_{\{P_k\}} + \dots + H_{\{P_{n-1}\}} + H_{\{P_n\}} \quad (1)$$

Terms like  $H_{\{P_k\}}$  contain rovibrational operators which have no matrix element within the  $P_{k' > k}$  basis sets. The effective Hamiltonian for polyad  $P_n$  is obtained by projecting  $H$  in the  $P_n$  Hilbert subspace, *i.e.*

$$H^{<P_n>} = P^{<P_n>} \mathcal{H} P^{<P_n>} = H_{\{GS\}}^{<P_n>} + H_{\{P_1\}}^{<P_n>} + \dots + H_{\{P_k\}}^{<P_n>} + \dots + H_{\{P_{n-1}\}}^{<P_n>} + H_{\{P_n\}}^{<P_n>} \quad (2)$$

The different terms are written in the form

$$\mathcal{H}_{(P_k)} = \sum_{all\ indexes} t_{\{S\}\{S'\}}^{\Omega(K,n\Gamma)\Gamma_v\Gamma'_v} \beta [V_{\{S\}\{S'\}}^{\Omega_v(\Gamma_v\Gamma'_v)\Gamma} \otimes R^{\Omega(K,n\Gamma)}]^{(A_1)} \quad (3)$$

In this equation, the  $t_{\{S\}\{S'\}}^{\Omega(K,n\Gamma)\Gamma_v\Gamma'_v}$  are the parameters to be determined, while  $V_{\{S\}\{S'\}}^{\Omega_v(\Gamma_v\Gamma'_v)\Gamma}$  and  $R^{\Omega(K,n\Gamma)}$  are vibrational and rotational operators of respective degree  $\Omega_v$  and  $\Omega$ . Their construction is described in Ref. [21]. Again, the vibrational operators only have matrix elements within the  $P_{k' \leq k}$  basis sets.  $\beta$  is a factor that allows the scalar terms ( $\Gamma = A_1$ ) to match the usual terms like  $B_0 J^2$ , *etc.* The order of each individual term is  $\Omega + \Omega_v - 2$ .

Such a Hamiltonian development scheme enables the treatment of any polyad system. The  $\nu_2$  and the  $\nu_4$  harmonic wavenumbers being close to each other, as mentioned above, we a priori consider that the two stretching fundamentals form a  $\nu_2/\nu_4$  dyad, just as for the  $OsO_4$  case [24]. Thus, we build up the following effective Hamiltonians:

- The ground state (polyad  $P_0$ ) effective Hamiltonian.

$$H^{<GS>} = H_{\{GS\}}^{<GS>} \quad (4)$$

- The  $\nu_2/\nu_4$  bending dyad ( $P_1$  effective Hamiltonian) effective Hamiltonian.

$$H^{<\nu_2/\nu_4>} = H_{\{GS\}}^{<\nu_1/\nu_3>} + H_{<\nu_2/\nu_4>}^{<\nu_2/\nu_4>} \quad (5)$$

A dipole moment operator for  $\nu_2/\nu_4$  is developed in the same way (see for instance [21] for details about its construction). In the present work, it is expanded at the minimum order for this stretching dyad, giving only one parameter which is the dipole moment derivative of  $\nu_4$  (see Section 4).

Here a vibrational basis restricted to the  $\nu_2$  and  $\nu_4$  modes is used:

$$|\Psi^{(X)}\rangle = |(\Psi_{\nu_2=1}^{(l_2=1,E)} \otimes \Psi_{\nu_4=1}^{(l_2=1,F_2)})\rangle \quad (6)$$

*i.e.* a three dimensional harmonic oscillator wavefunction for the triply degenerate mode  $\nu_4$  with vibrational angular momentum  $l_4$  and a two dimensional one for the mode  $\nu_2$  is used. The Hamiltonian and dipole moment matrix elements are calculated in the coupled rovibrational basis:

$$|[\Psi_v^{(C_v)} \otimes \Psi_r^{(J,nC_r)}]^{(C)}\rangle \quad (7)$$

$\Psi_r^{(J,nC_r)}$  is a rotational wavefunction with angular momentum  $J$ , rotational symmetry species  $C_r$  and multiplicity index  $n$  (see Ref. [19]), while  $C$  is the overall symmetry species ( $C = C_v \otimes C_r$ ).

#### 4. Analysis

Due to the overlap of the different isotopologue spectra, it is not possible to reliably assign lines with a natural abundance spectrum. Thus, an isotopically pure sample of  $^{102}\text{RuO}_4$  was studied, allowing much easier assignments. A preliminary simulation for  $^{102}\text{RuO}_4$  only was performed, using the XTDS software [25], which implements the formalism described in the previous section, starting from first guess Hamiltonian parameters, adapted from ref 7 and 24, and estimating first the Coriolis constants from the well-known sum rule and relations [28]. In particular, from ref 7, the Coriolis constant  $\xi_3$  could be determined as 0.1943, thus, since  $\xi_3 + \xi_4 \approx 0.5$ ,  $\xi_4 = 0.3057$  was taken as a starting value and thus a  $t_{\{4\}\{4\}}^{1(1,0F_1)} = 3\sqrt{2}B_4\xi_4 = 0.17598$  parameter value was assumed. In the following, the ground state effective Hamiltonian was expanded up to order zero only, since we have no precise spectroscopic ground state data. Unlike for  $\text{OsO}_4$ , we found no experimental gas phase spectroscopic determination of the bond length, but a recent X-Ray diffraction study of crystalline  $\text{RuO}_4$  exists [29]. The authors found two distinct crystalline phases, in which  $\text{RuO}_4$ , although distorted from tetrahedral symmetry, presents an average bond length of  $1.697 \pm 0.004 \text{ \AA}$ . The crystal structure has been obtained at low temperature (170K) and the bond distance should not be too different from that of the vibrational ground state. It has thus been used here as a starting point for the molecular equilibrium structure. The single ground state parameter used here, namely the  $B_0$  rotational constant, was therefore fixed to  $0.135794 \text{ cm}^{-1}$ , deduced from Ref. [29].

Due to the lack of references concerning intensities, we adapted manually an estimated value for the dipole moment parameter, in order to match roughly the experimental spectrum using the SPVIEW software [25].

Next, the  $\nu_4$  band center value was varied stepwise, to match approximately the onset of the strong Q branch in the  $335.5 \text{ cm}^{-1}$  vicinity. The general shape (contour, relative intensities) of the dyad was very understandably strongly dependent upon the energy interval between effective band centers and the extent of the Coriolis interaction. Again, since  $\xi_{24} = [\frac{1}{3}(1+2\xi_3)]^{1/2}$  in a first approximation [28],

a starting value of -0.292144 was assumed for the  $t_{\{2\}\{4\}}^{1(1,0F_1)} = -\frac{3}{2}\xi_{24}B_0(\sqrt{\frac{\nu_4}{\nu_2}} + \sqrt{\frac{\nu_2}{\nu_4}})$  parameter. As

will be seen later, the actual values for  $t_{\{4\}\{4\}}^{1(1,0F_1)}$  and  $t_{\{2\}\{4\}}^{1(1,0F_1)}$  depart only by -5 and +8 % from these starting guesses. For other parameters, the starting guesses were inspired by corresponding values in our  $^{192}\text{OsO}_4$  study [22-24], but vary more substantially.

Below  $320 \text{ cm}^{-1}$  the most prominent feature is the  $\nu_2$  Q-branch, constituted by relatively evenly spaced line clusters split by centrifugal effects. These clusters all correspond to relatively high  $J$  values ( $J \geq 20$ ) as the coupling and thus intensity transfer originates from a rotational Coriolis effect. The assignment of the first observable line cluster is by no means obvious and, in a first step, the band center positions and magnitude of the coupling parameters were varied manually, until the relative intensities and Q branch positions reproduced approximately the observation. At this point, the simulated spectrum could reproduce well enough the positions of the low  $J$  values transitions in the P and R-branches of the  $\nu_4$  so that lines could be assigned at low  $J$  values and the rotational and distortion constants, as well as band centers were fitted.

This led to better simulations and more lines could be assigned, with increasing  $J$  values. This procedure was repeated until no more lines could be assigned. The  $\nu_2/\nu_4$  effective Hamiltonian was finally expanded up to order 4 and 6, respectively. The results for the fitted effective Hamiltonian parameters are shown in Table 1. For  $\nu_2$  6 parameters, for  $\nu_4$  17 parameters and two interaction parameters were necessary. Attempts at increasing the Hamiltonian parameter order did not converge to meaningful values for the additional parameters introduced in the model.



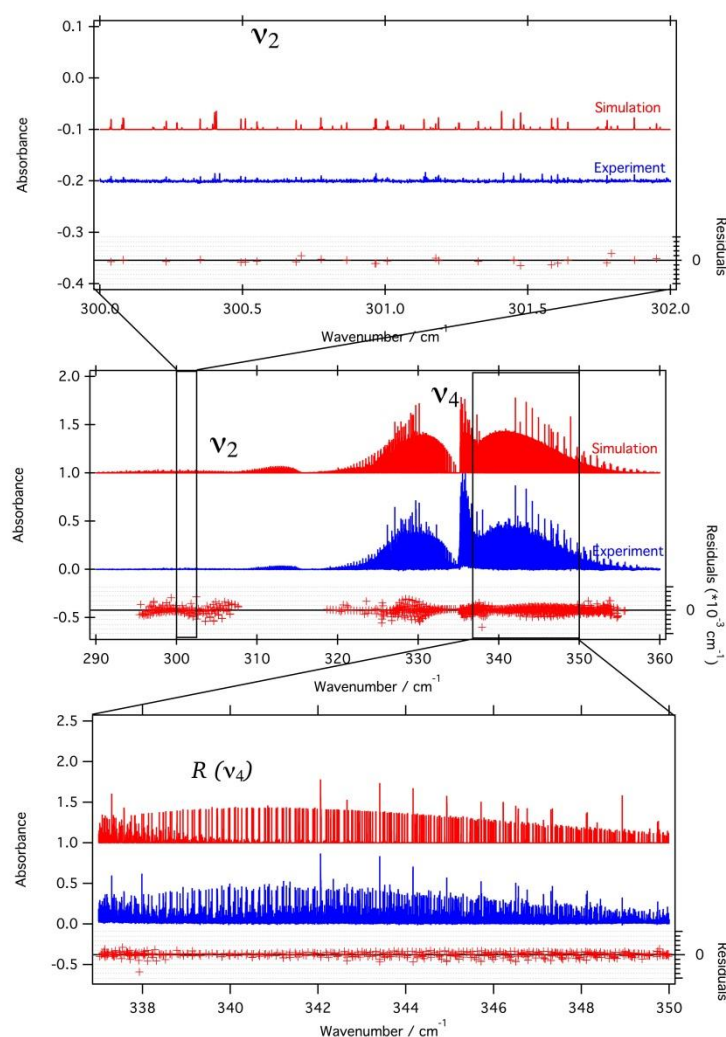


Figure 3: Top: Simulation of the  $\nu_2$  stretching mode of  $^{102}\text{RuO}_4$ , compared to the experiment. Middle: global view of the bending dyad, compared to the experiment. Bottom: detail in the  $R$  branch of the  $\nu_4$  region of  $^{102}\text{RuO}_4$ .

Finally, the obtained root mean square deviation ( $d_{\text{RMS}}$ ) is  $0.7 \times 10^{-3} \text{ cm}^{-1}$  for all 1037 assigned transitions ( $J_{\text{max}} = 88$ ). Fig. 3 shows a global comparison and  $P$ - and  $R$ - branch details between the simulation and the experimental spectrum of the  $^{102}\text{RuO}_4$ , while Fig. 4 show details in the  $\nu_2$  and  $\nu_4 Q$  branches.

It should be noted that the rotational resonance affecting the dyad is not entirely described by the model. In particular, when a good fit is obtained on the  $\nu_4$   $R$ -,  $Q$ - and first part ( $J < 26$ ) of the  $P$ -branches, as well as the  $P$  branch of the  $\nu_2$  itself, the simulations of the  $\nu_2$   $Q$ -branch and the closest part of the  $\nu_4$   $P$  branch presented as small offset, which could not be eliminated by adjusting any of the parameters here. While the model is successful at reproducing the broad picture (figure 4, top), it is clear that further refinement would be needed to account entirely of the spectrum in all details. Our attempts at correcting this using any of the effective Hamiltonian parameters listed were not successful and here other ground state parameters remain undetermined. As the bending levels are the lowest vibrational levels above the ground state, the closest vibrational states are combinations or overtones of these at about twice their energies, thus any vibrational resonance seems very unlikely. Perhaps a more complete modeling should include the  $\nu_3$  level as well, as a Coriolis coupling linking it with  $\nu_2$  can also exist. Given the large energy difference between  $\nu_2$  and  $\nu_3$  this was ignored here.



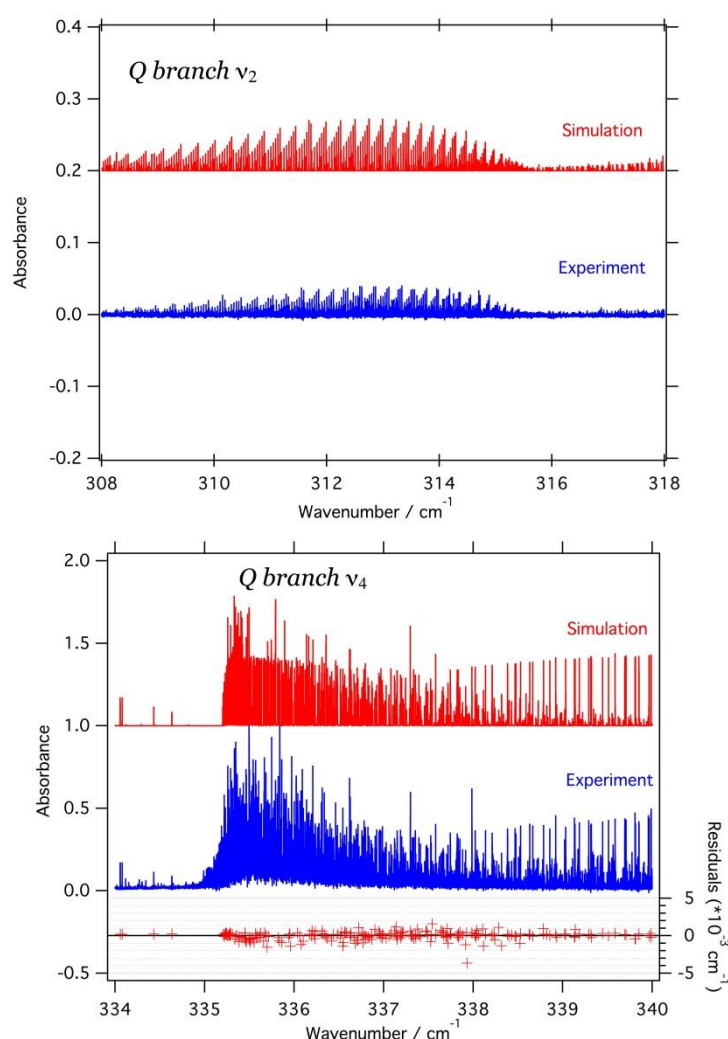


Figure 4: Detail in the Q branch of the  $\nu_4$  region of  $^{102}\text{RuO}_4$ , compared to the simulation.

## Conclusions

We have performed the first detailed FTIR high resolution spectroscopic investigation of the 300-350  $\text{cm}^{-1}$  bending region of  $^{102}\text{RuO}_4$ , the major isotopologue of ruthenium tetroxide. The spectrum was analyzed in detail. Our analysis covers the range of line assignments to high  $J$  values (88). The effective Hamiltonian parameters determined in this work will allow generating reasonable simulation for all  $\text{RuO}_4$  isotopologues, including the radioactive isotopologues  $^{103}\text{RuO}_4$  and  $^{106}\text{RuO}_4$ . The parameters and simulations can be obtained thanks to the XTDS software [25]. It has been updated with the present results and can be downloaded from the Dijon spectroscopy group's web page:

<http://icb.u-bourgogne.fr/departement/omr/spectroscopie-moleculaire-processus-collisionnels-et-applications/>

It is clear that this study leads to a more precise determination of the spectroscopic molecular parameters for the  $\nu_2$  and  $\nu_4$  vibrational modes of  $\text{RuO}_4$  (Table 1). A complete line list with attributions is available as supplementary material (S1). It is a first step on the way to a more precise structural parameters of this important benchmark molecule. This molecule poses also many challenging questions to ab initio quantum chemical calculations, as a recent study points out [14]. Among other properties, the predicted bond length varies substantially from one method to the next and is calculated always shorter. The predicted fundamental frequency ordering is also method-dependent [12 - 14]. The present study provides a very reliable estimate for the  $\nu_4$  fundamental band center, but the  $\nu_2$  is less precisely determined and might shift by some hundredths of wavenumbers if all interactions were taken into account.

## Acknowledgements

This work has been funded by the project DECA-PF "Investments for the future" program through ANR-11-RSNR-0003 grant, supervised by the "Agence Nationale pour la Recherche" under the "Research in Nuclear Safety and Radioprotection (RSNR)" initiative. We wish to thank Karine Chaouchi and Stéphanie Blanchandin (Soleil Chemistry support group) for their contribution in the sample synthesis.

## Bibliography

- [1] J. Beattie, Ruthenium-catalyzed homogeneous oxidation processes, *Pure and Applied Chemistry* **62**, p. 1145 (1990).
- [2] K. Masutani, T. Uchida, R. Irie, T. Katsuki, Catalytic asymmetric and chemoselective aerobic oxidation: kinetic resolution of sec-alcohols, *Tetrahedron Letters* **41(26)**, 5119 (2000)
- [3] J. Gatineau, K. Yanagita, C. Dussarrat, A new  $\text{RuO}_4$  solvent solution for pure ruthenium film depositions, *Microelectronic Engineering* (2006).
- [4] C. Mun, J. J. Ehrhardt, J. Lambert, C. Madic, XPS investigations of ruthenium deposited onto representative inner surfaces of nuclear reactor containment buildings, *Applied Surface Science* **253(18)**, 7613 (2007).
- [5] P. Giordano, A. Auvinen, G. Brilliant, J. Colombani, N. Davidovich, R. Dickson, T. Haste, T. Kärkelä, J.S. Lamy, C. Mun, D. Ohai, Y. Pontillon, M. Steinbrüci, N. Vér, Recent advances in understanding ruthenium behaviour under air-ingress conditions during a PWR severe accident, *Progress in Nuclear Energy* **52(1)**, 109 (2010).
- [6] P. Chatelard, N. Reinke, S. Arndt, S. Belon, L. Cantrel, L. Carenini, K. Chevalier-Jabet, F. Cousin, J. Eckel, F. Jacq, C. Marchetto, C. Mun, L. Piar, ASTEC V2 severe accident integral code main features, current V2.0 modelling status, perspectives, *Nuclear Engineering and Design* **272**, 119 (2014).
- [7] S. Reymond-Laruinaz, V. Boudon, L. Manceron, L. Lago, D. Doizi, Infrared Spectroscopy of Ruthenium Tetroxide and High-resolution analysis of the  $\nu_3$  band, *Journal of Molecular Spectroscopy* **315**, 46 (2015).
- [8] C.E. Düllmann, B. Eichler, R. Eichler, H. Gäggeler, A. Türkler, On the stability and volatility of group 8 tetroxides,  $\text{MO}_4$  (M= Ru, Os and Hs), *The Journal of Physical Chemistry B* **106**, 6678 (2002).

- [8] M. Filatov, D. Cremer, Calculation of electric properties using regular approximation to relativistic effects: the polarizabilities of RuO<sub>4</sub>, OsO<sub>4</sub> and HsO<sub>4</sub>, *The Journal of Chemical Physics* **119**, 1412 (2003).
- [9] V. Pershina, T. Bastug, B. Fricke, Relativistic effects on the electronic structure and volatility of group 8 tetroxides MO<sub>4</sub>, where M=Ru, Os and Hs, *The Journal of Chemical Physics* **122**, 124301 (2005).
- [10] M. Filatov, D. Cremer, A gauge-independent zeroth order regular approximation to the exact relativistic Hamiltonian-formulation and applications, *The Journal of Chemical Physics* **122**, 044104 (2005).
- [11] H. Hameka, J. Jensen, J.G. Kay, C.M. Rosenthal, G.L. Zimmerman, Theoretical predictions of geometries and vibrational infrared spectra of ruthenium oxide molecules, *Journal of Molecular Spectroscopy* **150**, 218 (1991).
- [12] P. Carbonnière, I. Ciofini, C. Adamo, C. Pouchan, Vibrational behavior of tetrahedral d<sup>0</sup> oxo-compounds: A theoretical study, *Chemical Physics Letters* **429**, 52 (2006).
- [13] L. Jose, M. Seth, T. Ziegler, Molecular and Vibrational Structure of Tetroxo d<sup>0</sup> Metal Complexes in their Excited States. A Study Based on Time-Dependent Density Functional Calculations and Franck–Condon Theory, *The Journal of Physical Chemistry A* **116**, 1864 (2012).
- [14] F. Miradji, S. Souvi, L. Cantrel, F. Louis, V. Vallet, Thermodynamic Properties of Gaseous Ruthenium Species, *Journal of Physical Chemistry A*, 119 4961 (2015).
- [15] I.W. Levin, Low-temperature Raman spectra of solid osmium tetroxide and ruthenium tetroxide, *Inorganic Chemistry* **8(4)**, 1018 (1969).
- [16] R. S. McDowell, L. B. Asprey, L. Claron Hoskins, Vibrational Spectrum and Force Field of Ruthenium Tetroxide, *The Journal of Chemical Physics* **56(11)**, 5712 (1972).
- [17] Marcel Snels, Maria Paola Sassi, Martin Quack, High-resolution Fourier-transform infrared spectroscopy of the ν<sub>3</sub>(F<sub>2</sub>) fundamental of RuO<sub>4</sub>, *Molecular physics* **72(1)**, 145 (1991).
- [18] J.P. Champion, M. Loëte, G. Pierre, Spherical top spectra, K.N. Rao, A. Weber (Eds.), *Spectroscopy of the Earth's atmosphere and interstellar medium*, Academic Press, San Diego, p. 339–422 (1992).
- [19] V. Boudon, J.P. Champion, T. Gabard, M. Loëte, F. Michelot, G. Pierre, et al., Symmetry-adapted tensorial formalism to model rovibrational and rovibronic spectra of molecules pertaining to various point groups, *Journal of Molecular Spectroscopy* **228**, 620 (2004).
- [20] A. Robiette, D. Gray, F. Birss, The effective vibration-rotation Hamiltonian for triply-degenerate fundamentals of tetrahedral XY<sub>4</sub> molecules, *Molecular Physics* **32(6)**, 1591 (1976).
- [21] C. Wenger, V. Boudon, M. Rotger, M. Sanzharov, J.P. Champion, XTDS and SPVIEW: graphical tools for the analysis and simulation of high-resolution molecular spectra, *Journal of Molecular Spectroscopy* **251(1–2)**, 102 (2008).

- [22] M. Louvriot, V. Boudon, L. Manceron, P. Roy, D. Balcon, High resolution spectroscopy and analysis of the  $\nu_1/\nu_3$  stretching dyad of osmium tetroxide, *Journal of Quantitative Spectroscopy and Radiative Transfer* **113**, 119 (2011).
- [23] M. Louvriot, V. Boudon, D. Bermejo, R. Martinez, L. Manceron, High resolution stimulated Raman spectroscopy and analysis of the  $\nu_1$  band of osmium tetroxide. *Journal of Raman Spectroscopy* **43(11)** (2012).
- [24] M. Louvriot, V. Boudon, L. Manceron, P. Roy, D. Bermejo, R. Martinez, High resolution spectroscopy and structure of osmium tetroxide: a benchmark study on  $^{192}\text{OsO}_4$ , *Inorganic Chemistry* **51**, 10356 (2012).
- [25] O. Ruff, E. Vidic, Wertigkeit des Rutheniums, Rutheniumtetroxyd und Ruthenium halogenid, *Zeitschrift für Anorganische und Allgemeine Chemie* **136**, 49 (1924).
- [26] A. B. Nikolskii, Saturated vapor pressure of ruthenium tetroxide, *Russian Journal of Inorganic Chemistry* **8**, 541 (1963).
- [27] L.S. Rothman, D. Jacquemart, A. Barbe, D.C. Benner, M. Birk, L.R. Brown, M.R. Carleer, C. Chackerian, K. Chance, L. Coudert, V. Dana, V. Malathy-Devi, J.M. Flaud, R.R. Gamache, A. Goldman, J.M. Hartmann, K.W. Jucks, A.G. Maki, J.Y. Mandin, S. Massie, J. Orphal, A. Perrin, C.P. Rinsland, M.A. Smith, R.A. Toth, J. Vander Auwera, P. Varanasi and G. Wagner, The HITRAN 2004 molecular spectroscopic database., *Journal of Quantitative Spectroscopy and Radiative Transfer* **96**, 139 (2005).
- [28] J.H.Meal, S.R.Polo *The Journal of Chemical Physics* **24**,1119 (1956).
- [29] M.Pley, M.S. Wickleder, *Journal of Solid State Chemistry*. 178, 3206 (2005). Two crystalline modifications of  $\text{RuO}_4$ .
- [30] J.K. Watson, *Journal of Molecular Spectroscopy* **39(2)**, 364 (1971). Quadratic Coriolis Zeta sum rules.
-

Table 1: Effective Hamiltonian Parameters for the  $\nu_2/\nu_4$  dyad of  $\text{RuO}_4$ . Uncertainty is indicated in parentheses, in the unit of the last two digits. Only fitted parameters are reported

Band	Order	$\Omega$ (K, n $\Gamma$ )	Parameters		Values / $\text{cm}^{-1}$ (1 $\sigma$ St. Dev.)	"Usual" notation
			{s}	{s'}		
$\nu_2$	0	0(0,0A1)	0100E	0100E	315.82914(62)	$\nu_2$
	2	2(0,0A1)	0100E	0100E	$2.440(38) \times 10^{-4}$	$B_2-B_0$
	2	2(2,0E )	0100E	0100E	$2.082(33) \times 10^{-4}$	
	3	3(3,0A2)	0100E	0100E	$3.1(1.2) \times 10^{-8}$	
	4	4(0,0A1)	0100E	0100E	$4.66(30) \times 10^{-9}$	
	4	4(2,0E )	0100E	0100E	$-7.03(15) \times 10^{-9}$	
$\nu_4-\nu_2$	1	1(1,0F1)	0100E	0001F2	$-3.1843(53) \times 10^{-1}$	$\nu_4-\nu_2$ interaction
	2	2(2,0F2)	0100E	0001F2	$-2.402(16) \times 10^{-4}$	
$\nu_4$	0	0(0,0A1)	0001F2	0001F2	335.28053(11)	$\nu_4$
	1	1(1,0F1)	0001F2	0001F2	$1.67321(10) \times 10^{-1}$	$3\nu_2 B_2 \zeta_3$ (Coriolis $\nu_4$ )
	2	2(0,0A1)	0001F2	0001F2	$-1.747(25) \times 10^{-4}$	$B_4-B_0$
	2	2(2,0E )	0001F2	0001F2	$3.239(37) \times 10^{-4}$	
	2	2(2,0F2)	0001F2	0001F2	$-2.516(27) \times 10^{-4}$	
	3	3(1,0F1)	0001F2	0001F2	$0(1.1) \times 10^{-8}$	$(3\nu_3/4\nu_2) F_{110}^3$
	3	3(3,0F1)	0001F2	0001F2	$6.9(1.0) \times 10^{-8}$	$(3/\nu_5/2) F_{134}^3$
	4	4(0,0A1)	0001F2	0001F2	$-3.58(17) \times 10^{-9}$	$-(D_4-D_0)$
	4	4(2,0E )	0001F2	0001F2	$-1.7(1.4) \times 10^{-10}$	
	4	4(2,0F2)	0001F2	0001F2	$-1.9(1.3) \times 10^{-10}$	
	4	4(4,0A1)	0001F2	0001F2	$7.0(1.5) \times 10^{-11}$	
	4	4(4,0E )	0001F2	0001F2	$-3.067(51) \times 10^{-9}$	
	4	4(4,0F2)	0001F2	0001F2	$-1.050(61) \times 10^{-9}$	
	5	5(1,0F1)	0001F2	0001F2	$-7.42(45) \times 10^{-12}$	
	5	5(3,0F1)	0001F2	0001F2	$5.23(49) \times 10^{-12}$	
	5	5(5,0F1)	0001F2	0001F2	$4.01(21) \times 10^{-12}$	
	5	5(5,1F1)	0001F2	0001F2	$-2.792(60) \times 10^{-11}$	
	6	6(0,0A1)	0001F2	0001F2	$-1.48(85) \times 10^{-14}$	

